energies

MDPI

Article

Effects of MgO Nanoparticles on Thermo-Physical Properties of $LiNO_3$-$NaNO_3$-KNO_3 for Thermal Energy Storage

Jianfeng Lu [1,*], Zhan Zhang [2], Weilong Wang [1] and Jing Ding [1,*]

[1] School of Materials Science and Engineering, Sun Yat-Sen University, Guangzhou 510006, China; wwlong@mail.sysu.edu.cn
[2] School of Intelligent Systems Engineering, Sun Yat-Sen University, Guangzhou 510006, China; zhangzh95@mail2.sysu.edu.cn
* Correspondence: lujfeng@mail.sysu.edu.cn (J.L.); dingjing@mail.sysu.edu.cn (J.D.)

Abstract: Molten salt $LiNO_3$-$NaNO_3$-KNO_3 has been investigated as heat transfer and thermal storage media for its low melting point and good thermal performance. In this paper, nanofluids were synthesized by dispersing MgO nanoparticles into $LiNO_3$-$NaNO_3$-KNO_3, and the effects of nanoparticles on thermal properties were studied with different sizes (20–100 nm) and mass percent concentrations (0.5–2.0 wt.%). The addition of nanoparticles had little effect on melting temperature, and led to a slight increase in enthalpy of fusion by 2.0–5.5%. Compared with base salt, the density of nanofluid increased a little by 0.22–1.15%. The scanning electron microscope (SEM) test implied that nubby and punctate microstructures were responsible for larger surface area and interfacial energy, which could lead to the improvement of specific heat capacity reaching 2.6–10.6%. The heat transfer characteristics remarkably increased with the addition of nanoparticles, and the enhancement of average thermal diffusivity and conductivity of salt with 1 wt.% nano-MgO could be 5.3–11.7% and 11.3–21.2%, respectively. Besides, the viscosities of nanofluids slightly increased for 3.3–8.1%. As a conclusion, nano-MgO was positively influential on the thermal properties of $LiNO_3$-$NaNO_3$-KNO_3 base salt.

Keywords: thermal energy storage; ternary nitrate salt; nanofluid; thermal properties

Citation: Lu, J.; Zhang, Z.; Wang, W.; Ding, J. Effects of MgO Nanoparticles on Thermo-Physical Properties of $LiNO_3$-$NaNO_3$-KNO_3 for Thermal Energy Storage. *Energies* **2021**, *14*, 677. https://doi.org/10.3390/en14030677

Academic Editor: Andrea Frazzica
Received: 22 December 2020
Accepted: 25 January 2021
Published: 28 January 2021

1. Introduction

The increasing population and challenge of environment crisis compel the development of large-scale renewable resources and clean energy technologies. To explore feasible solutions, numerous researchers have paid much attention to solar energy, especially concentrating solar power (CSP) with thermal energy storage (TES) [1]. Due to the advantages of excellent thermal properties and ideal economy, molten salts are generally utilized as heat transfer and thermal storage media. Solar Salt and Hitec salt are commonly researched in all aspects to meet the application requirements [2].

Molten salts have considerable foregrounds for thermal characteristics enhancement, and doping nanoparticles into base salt is a resulting method to increase specific heat capacity and thermal conductivity. Several nanoparticles, including SiO_2, TiO_2, Al_2O_3, CuO, and MgO, are usually doped as desired additives. Dudda and Shin [3] doped 1 wt.% SiO_2 nanoparticles with sizes of 5–60 nm into Solar Salt, and the specific capacity could be enhanced by 8–24% in the liquid phase, which revealed that the nanostructures were mainly responsible for the reinforcement of specific capacity. Ho and Pan [4] experimentally dispersed 50 nm Al_2O_3 nanoparticles with different mass percent concentrations (0.016, 0.063, and 0.125 wt.%) in HITEC, and the greatest enhancement of specific capacity was gained with the optimum concentration of 0.063 wt.%. According to previous studies [5,6], the addition of nanoparticles could take the shape of fractal-like nanostructures and solid-like nanolayers, and it was the great specific surface area that resulted in the increasement of surface energy and specific capacity. As for the heat transfer characteristics,

Wei et al. [7] synthesized nanomaterials with different mass percent concentrations of MgO nanoparticles to enhance the thermo-physical properties of Solar Salt, and found that the reinforcement of thermal conductivity could exceptionally reach by 62.1% with 5 wt.% nano-MgO additions, indicating that MgO-nanoparticles were superior additives. Nithiyanantham et al. [8] investigated the shape effect of Al_2O_3 nanoparticles on thermo-physical properties of a binary nitrate molten salt with two different shapes (nanospheres and nanorods), and reported that the enhancement of thermal conductivity with nanoparticles at 400 °C could reach 16%, which was obviously higher than 12% of nanorods. Based on earlier literature [9,10], there are two main factors that contribute to the enhancement of thermal conductivity: the formation of the nanostructure and the Brownian motion.

In practical applications, the utilization of molten salt media with a low melting temperature can effectively reduce the risk of blockage in pipelines and improve the safety and stability of the apparatus. Recently, ternary nitrate molten salt $LiNO_3$-$NaNO_3$-KNO_3 has been investigated as heat transfer and thermal storage media considering its low melting point and good thermal performance [11]. Coscia et al. [12] experimentally measured the enthalpy of fusion, specific heat capacity, and viscosity of $LiNO_3$-$NaNO_3$-KNO_3, and concluded that it could be a good candidate as a heat transfer fluid for CSP. Wang et al. [13] used a simplified inverse method to measure the thermal conductivity of $LiNO_3$-$NaNO_3$-KNO_3 in the solid state. Seo and Shin [14] dispersed 1 wt.% nano-SiO_2 with different sizes (5–60 nm) into $LiNO_3$-$NaNO_3$-KNO_3, and reported that specific capacity could be enhanced by 13–16%.

Till now, the enhancement of thermophysical properties for $LiNO_3$-$NaNO_3$-KNO_3 has not been sufficiently studied in available literature. In this paper, thermophysical properties of $LiNO_3$-$NaNO_3$-KNO_3 with MgO nanoparticles were investigated with different mass percent concentrations (0.5–2.0 wt.%) and sizes (20–100 nm). The effects of nanoparticles on thermophysical properties including melting temperature, enthalpy of fusion, specific heat capacity, density, viscosity, thermal diffusivity, and thermal conductivity were reported and analyzed. In additional, the enhanced mechanism of specific heat capacity and thermal conductivity was examined by scanning electron microscope (SEM) and literature references.

2. Materials and Methods

2.1. Preparation of Base Salt and Nanofluids

The ternary nitrate molten salt $LiNO_3$-$NaNO_3$-KNO_3 (37.5%-9.0%-53.5%, mol.%) was prepared by static melting method [15]. Lithium nitrate (A.R.) was gained from Shanghai Aladdin Biochemical Technology Co. Ltd. (Shanghai, China), and sodium nitrate (A.R.) and potassium nitrate (A.R.) were received from Guangzhou Chemical Reagent Technology Co. Ltd. (Guangzhou, China). Firstly, to prevent moisture, the raw materials were held in a drying oven at 120 °C for 24 h beforehand. Then three kinds of nitrates of corresponding masses were taken separately. In order to reduce the bubble generation in the liquid salt, the nitrates were manually stirred by a quartz bar in a corundum crucible until no lumps appeared. Next, the mixture was heated from ambient temperature to 350 °C with a heating rate of 5 °C/min in a muffle furnace, and held at 350 °C for 10 h to eliminate bubbles and form a homogeneous mixture. In the end, it was poured into a stainless tray, cooled at ambient temperature, ground into powder, and kept sealed in a desiccator.

MgO-nanoparticles of different average sizes were purchased from Shanghai Naiou Nano Technology Co. Ltd (Shanghai, China). with a purity of 99.9%. In order to ensure the size and uniformity, nanoparticles were observed by scanning electron microscopy (SEM, Zeiss-G500, Oberkochen, Germany). The microtopography results of 20 and 100 nm nanoparticles as examples are shown in Figure 1. From SEM micrograph, nanoparticles were spherical, about 20 and 100 nm in average diameter, and evenly distributed. It indicated the nanoparticles were not spoiled by moisture and could meet the experimental standards.

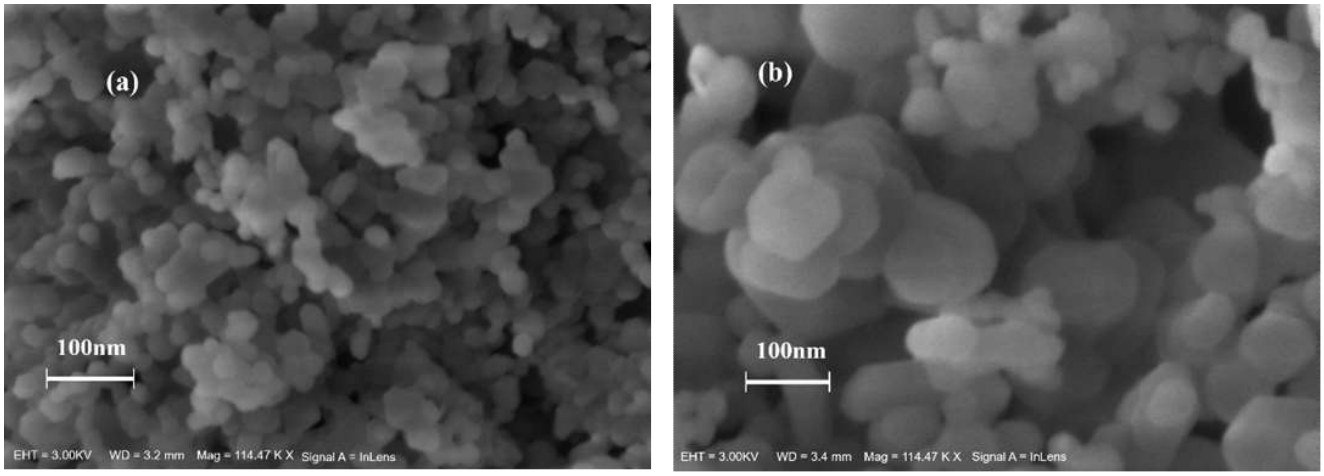

Figure 1. SEM image of MgO nanoparticles: (**a**) average size of 20 nm; (**b**) average size of 100 nm.

Nanofluids were prepared by "two-step method" [7]. The nanofluids containing a ternary base salt and nano-MgO of different sizes (20, 40, 60, 100 nm) and mass percent concentrations (0.5%, 1.0%, 1.5%, 2.0%) were prepared by mechanical agitation method. First of all, the prepared base salt was heated to 350 °C with a heating rate of 5 °C/min in a muffle furnace, held at 350 °C for 3h, and stabilized in liquid phase. Afterwards, MgO-nanoparticles of different sizes or mass percent concentrations were added into base salt at 350 °C. Then a quartz bar fixed on a metal frame was inserted into the liquid mixture and mechanically stirred with 120 rpm for 1 h. When a homogeneous MgO dispersed nanofluid was formed at high temperature, it was held at 350 °C for 5 h to remove the bubbles. Similar to the operation of base salt, nanofluids were poured out, ground to powder, sealed in a drying oven for subsequent experiments.

2.2. Characterization Techniques

The enthalpy of fusion and melting temperature were determined by differential scanning calorimeter (DSC 404 F3) from Germany NETZSCH Company (Selb, Germany). In the first place, six reference metal materials (In, Sn, Pb, Zn, Al, Au) should be calibrated to ensure the accuracy of sensitivity and temperature. The calibration results guaranteed the temperature uncertainty within ±2 K and enthalpy uncertainty within 3%. Graphite crucibles were used to hold samples to be tested (approximate 5–15 mg). Besides, the experiments were carried out under an argon atmosphere with a flow rate of 50 mL/min and at a heating rate of 10 °C/min. The salt samples were first heated to 100 °C from ambient temperature and held for 5min to remove the moisture. After that, samples were heated to 170 °C and held for 5min. Then samples were cooled at 50 °C, and held for 5 min. Finally, the operation was repeated again for another measurement.

Specific heat capacity was also characterized by DSC (404 F3, Selb, Germany). After the calibration of reference metal materials, the uncertainty can be confirmed within 5%. Based on sapphire method, the heat flow curves of blank crucible as blank baselines, sapphire as a standard sample, and molten salts (approximate 40 mg, the same mass with sapphire) were, respectively, measured under an argon atmosphere with a flow rate of 50 mL/min and at a heating rate of 10 °C/min. Specific heat capacity of salt sample can be obtained by three DSC curves as the following Equation,

$$c_{p,\mathrm{salt}} = \frac{q_{\mathrm{salt}} - q_{\mathrm{base}}}{q_{\mathrm{ref}} - q_{\mathrm{base}}} \times \frac{c_{p,\mathrm{ref}} \times m_{\mathrm{ref}}}{m_{\mathrm{salt}}} \quad (1)$$

where q_{salt}, q_{ref}, and q_{base} represent the DSC curve signals of the salt, sapphire, and empty crucible. $c_{p,\mathrm{salt}}$ and $c_{p,\mathrm{ref}}$ are the specific heat capacities of the salt and reference material (sapphire). m_{salt} and m_{ref} are the masses of salt and sapphire, respectively.

Based on Archimedean theory, the molten salt synthetic apparatus was set up to gain the density of sample, whose uncertainty is less than 1%. The weights of platinum hammer in air, water, and molten salt were measured, respectively. The density of the molten salt can be expressed as:

$$\rho = \frac{m_a - m_s}{V_p[1 + \alpha_{(pt)}(t - 25)]^3} \quad (2)$$

where the V_p is the volume of the platinum hammer, m_a and m_s are, respectively, weights of the platinum hammer in the air and liquid molten salt. $\alpha_{(pt)}$ represents the linear expansion coefficient of the platinum. The measurements were carried out from 160 to 370 °C and with an argon flow (100 mL/min).

The integrated viscosity measuring device purchased from Shanghai Yuzhi Electrical Mechanical Equipment Co. Ltd (Shanghai, China). was employed to gain the viscosity, and the viscometer was from Brookfield (RVDV-2T, Massachusetts, America). Based on the coaxial cylinder method, a stainless steel crucible holding salt sample about 100 mL was fixed on a shelf, and they were placed in a muffle furnace. Salt sample was measured with the temperature range from 160 to 370 °C, flow rate of 100 mL/min and an argon atmosphere as protective gas, which can take away the volatile gas from the salt sample and protect the equipment. The rotor immersed in the liquid salt rotated with a rotor speed of 30 rpm, and the uncertainty of this instrument can be guaranteed within 0.2 cP.

Laser flash analysis (LFA 1000, Linseis, Selb, Germany) was utilized to obtain the thermal diffusivity of liquid salt sample, and its uncertainty is less than 7%. Samples of 1.8 g were placed in a specially designed graphite crucible, heated from ambient temperature to 180 °C, held for another 2 h, and then cooled to 100 °C. This procedure should be repeated three times in order to eliminate the interference of bubbles in the liquid and to form a sample of uniform thickness. The experiment should be conducted under an argon atmosphere (100 mL/min) and with a heating rate of 2 °C min. The result of thermal diffusivity at each target temperature was taken as an average of four laser pulses at least. According to Parker's Equation, the thermal diffusivity was described as:

$$\alpha = 0.1338\frac{l^2}{t_{0.5}} \quad (3)$$

where l is the thickness of the liquid, and $t_{0.5}$ is half the time it takes for the laser pulse to reach the upper surface of the liquid sample and rise to steady state.

The thermal conductivity was calculated as:

$$\lambda = \alpha \cdot \rho \cdot c_p \quad (4)$$

and the uncertainty of the thermal conductivity can be calculated by the following Equation:

$$\frac{S_\lambda}{\lambda} = \sqrt{\left(\frac{\partial \ln \lambda}{\partial \rho}\right)^2 S_\rho^2 + \left(\frac{\partial \ln \lambda}{\partial c_p}\right)^2 S_{c_p}^2 + \left(\frac{\partial \ln \lambda}{\partial \alpha}\right)^2 S_\alpha^2} = \sqrt{\left(\frac{S_\rho}{\rho}\right)^2 + \left(\frac{S_{c_p}}{c_p}\right)^2 + \left(\frac{S_\alpha}{\alpha}\right)^2} \quad (5)$$

where the uncertainties of density, specific heat capacity, and thermal diffusivity were obtained in the above, so the uncertainty of thermal conductivity was 8.7%.

The thermal properties are closely related to microstructures, so scanning electron microscopy (SEM, Zeiss-G500, Oberkochen, Germany) was employed to perform the characterization analyses of ternary nitrate base salt and nanofluids, respectively. The combination (1 wt.%, 20 nm) providing the highest specific heat capacity enhancement would be chosen to be tested as an example. By comparing with the micrographs, the enhancement mechanism on properties can be determined.

3. Results and Discussion

3.1. Melting Temperature and Enthalpy of Fusion

Figure 2 shows the DSC curves and the melting temperature and enthalpy of fusion of nanofluids with different sizes and mass percent concentrations, respectively. It demonstrated that the addition of nanoparticles had little effect on the melting point of $LiNO_3$-$NaNO_3$-KNO_3, but led to a slight increase in enthalpy of fusion, whose improvement could reach 2.0–5.5%. According to literature studies [16,17], nanoparticles will aggregate in base salts to some extent. In order to reach a stable state, the system needs more energy to disperse these clusters, which will result in the increase of enthalpy of fusion. Besides, the increase of nanoparticles aggregation will lead to the decrease of interfacial energy, which could result in the decrease of enthalpy of fusion. Under the combined effects of the two factors, when the mass percent concentration of nanoparticles was 2.0 wt.%, the increase of enthalpy of fusion was the smallest.

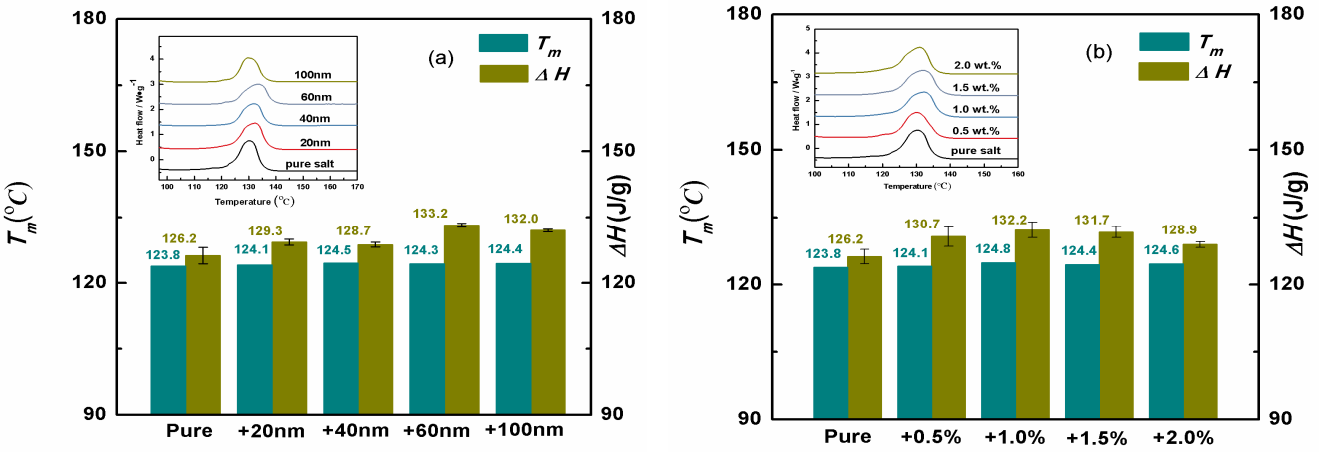

Figure 2. DSC curves and effects of MgO nanoparticles on the melting temperature and enthalpy of fusion: (**a**) different sizes (1.0 wt.%); (**b**) different mass percent concentrations (20 nm).

3.2. Enhanced Specific Heat Capacity

Specific heat capacity is an extremely important parameter that reflects heat storage capacity. The specific heat capacity results of nanofluids with different nano particle sizes and mass percent concentrations are depicted in Figure 3, whose mean relative experimental error was about 1.49%. From the graphs, the specific heat capacity of $LiNO_3$-$NaNO_3$-KNO_3 markedly increased by 2.6–10.6% with the addition of nano-MgO, and the maximum enhancement occurred when 1.0 wt.% nano-MgO (20 nm) was dispersed. Besides, with the increase of temperature, the specific heat capacity mildly decreased by about 6.6%.

The classical mixing theory [18] for specific heat capacity of mixture can be expressed as:

$$c_{p,\mathrm{nf}} = \frac{m_\mathrm{b} c_{p,\mathrm{b}} + m_\mathrm{np} c_{p,\mathrm{np}}}{m_\mathrm{nf}} \quad (6)$$

where $c_{p,\mathrm{nf}}$, $c_{p,\mathrm{b}}$, and $c_{p,\mathrm{np}}$ are the specific heat capacities of nanofluids, base salt, and nanoparticles, and m_nf, m_b, and m_np represent the mass of nanofluids, base salt, and nanoparticles, respectively. According to literature reference [7], the specific heat capacity of MgO is 1.18 J/g·°C and lower than 1.485 J/g·°C of the base salt. From 190 to 340 °C, the average specific heat capacity of nanofluids with 1 wt.% nano-MgO (20 nm) was 1.642 J/g·°C. The specific heat capacity of nanofluids calculated by mixing theory was 1.482 J/g·°C, which was remarkably lower than experimental data, indicating that the classical mixing theory failed to give a reasonable explanation for the enhancement of specific heat capacity.

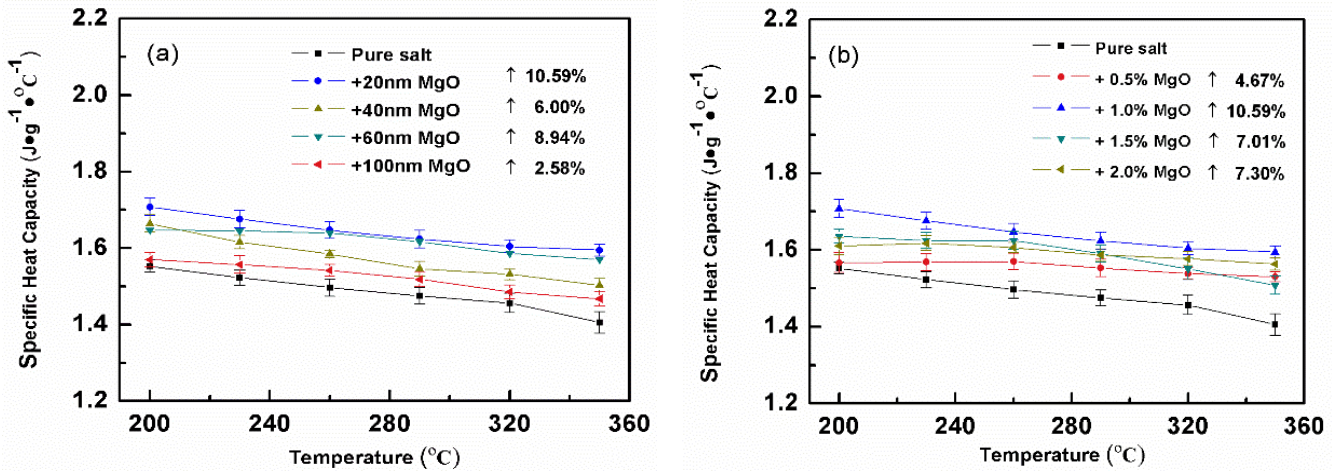

Figure 3. Effects of MgO nanoparticles on the specific heat capacity: (**a**) different sizes (1 wt.%); (**b**) different mass percent concentrations (20 nm).

The morphology of base salt and nanofluid was observed at the micro level by scanning electron microscopy (SEM) as shown in Figure 4, and the combination (1.0 wt.%, 20 nm) providing the highest specific heat capacity enhancement was chosen as an example. The surface of base ternary nitrate salt was very smooth without any special structures. In the nanofluids, there were nubby and punctate microstructures. Some exceptionally fine nanoparticles of MgO evenly attached to the surface of base salt, which could bring the increase of surface area and then led to the tremendous interfacial energy and better thermal storage performance [7]. From Figure 3, it could be seen that the combination of 20 nm 1.0 wt.% was the optimal dispersion, and the nanoparticles in this case can bring the largest available surface area [19].

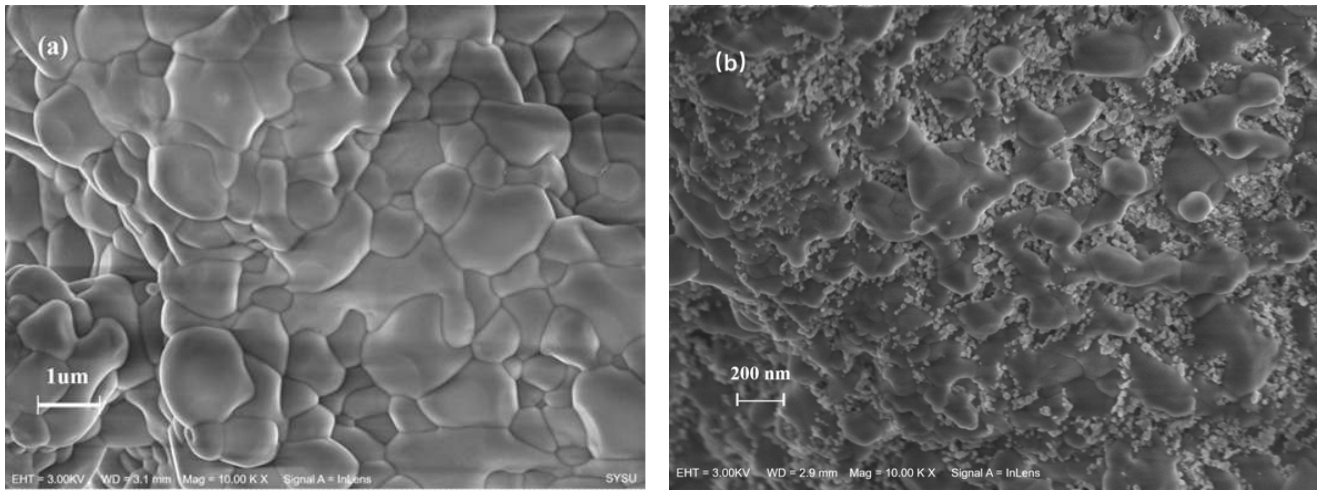

Figure 4. SEM images of: (**a**) pure ternary nitrate salt; (**b**) nanofluids (20 nm-MgO of 1 wt.%).

3.3. Density

The densities of nanofluids are depicted in Figure 5, whose mean relative experimental error was about 0.19%. For all groups of tests, densities linearly decreased with increasing temperature. Nanoparticles could slightly increase the density of $LiNO_3$-$NaNO_3$-KNO_3 with a maximum increase of 1.15% (1 wt.%, 100 nm). According to densities of nanofluids with different fractions in Figure 5b, the weakest and the most pronounced enhancement

occurred at 0.5 and 2.0 wt.%, respectively. With the nano size of 20 nm, when 2.0 wt.% particles were added, the enhancement of density could reach by 0.92% at most.

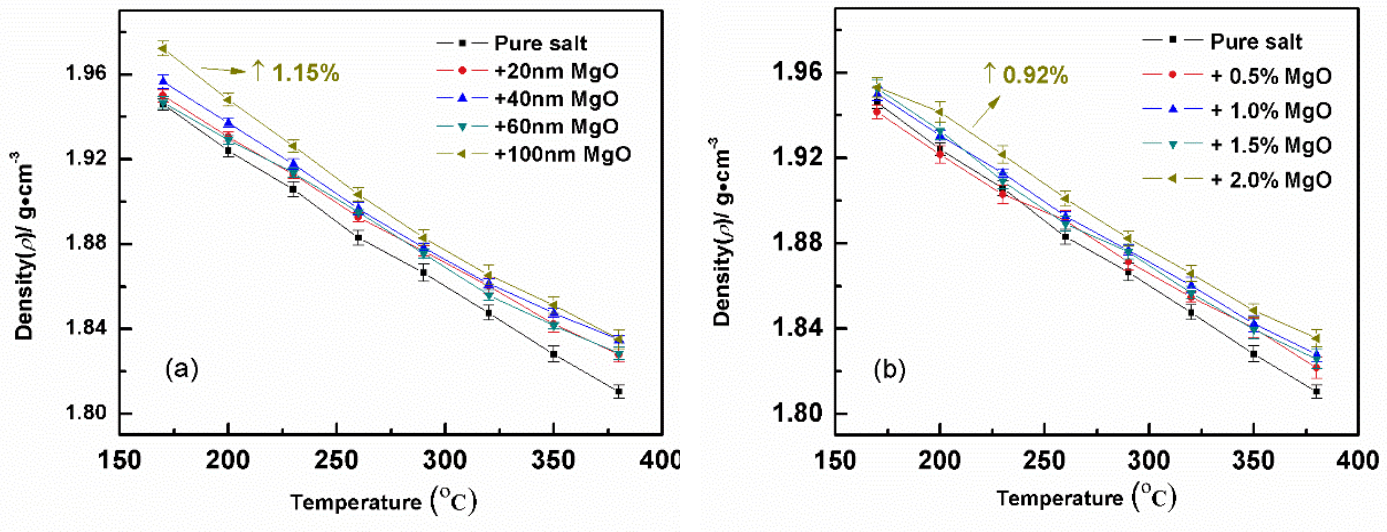

Figure 5. Effects of MgO nanoparticles on the density: (**a**) different sizes (1 wt.%); (**b**) different mass percent concentrations (20 nm).

3.4. Viscosity

The effects of nano sizes and mass percent concentrations on nanofluid viscosity are shown in Figure 6, and the mean relative experimental error was about 3%. When 1.0 wt.% nano-MgO of different sizes were dispersed, the improvement of nanofluid viscosity was 3.3–4.9%, so nano size made little difference on the improvement results. The improvement effects of nanofluid viscosity became more obvious with the increase of mass percent concentration. When mass percent concentration was from 0.5 to 2.0 wt.%, nanofluid viscosity with 20 nm-MgO reached by 3.4–8.1%, and this trend was in good agreement with that of Solar Salt with nano-SiO_2 [20]. Although the viscosity increased slightly with the addition of nanoparticles, it was still close to that of Solar Salt.

3.5. Enhanced Thermal Diffusivity

In consideration of the greatest enhancement of specific heat capacity, nano-MgO with the mass percent concentration of 1 wt.% was chosen to estimate the effects of nanoparticles on the heat transport performance. The thermal diffusivities of nanofluids are shown in Figure 7, whose mean relative experimental error was about 4.2%. The thermal diffusivity can be improved by adding minute quantities of nano-MgO to the base salt, and it increased with the temperature rising. The thermal diffusivity enhancement of nanofluids with different particle sizes (20–100 nm) in 220–340 °C could reach by 5.3–13.7%. When 40 nm nano-MgO was dispersed, the enhancement of thermal diffusivity can reach 13.7% to the utmost.

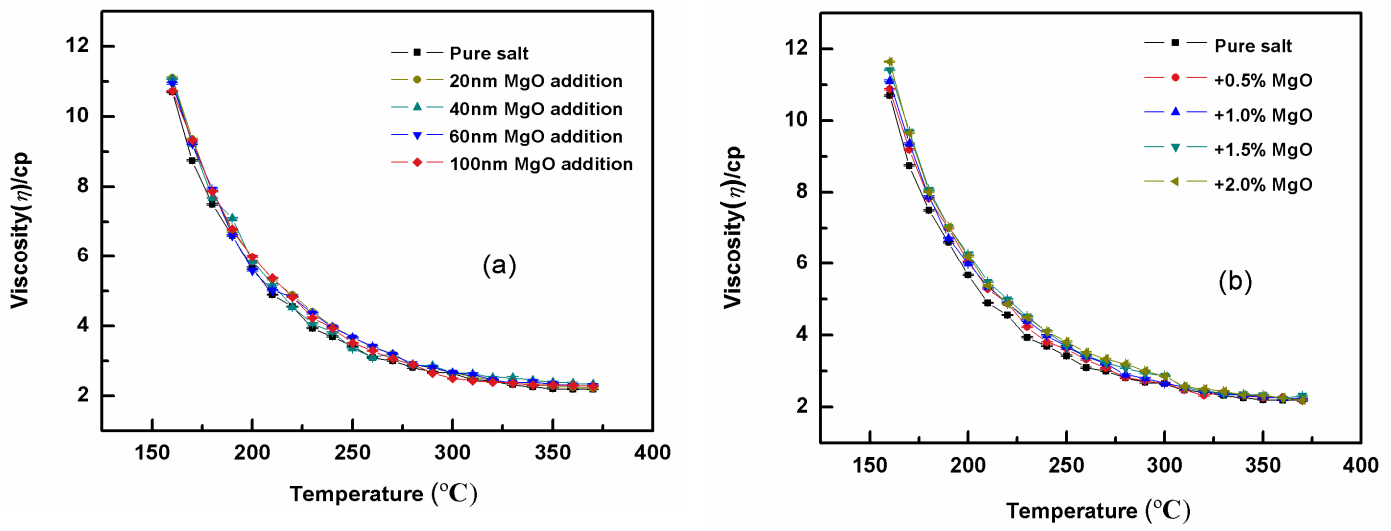

Figure 6. Effects of MgO nanoparticles on the viscosity: (**a**) different sizes (1 wt.%); (**b**) different mass percent concentrations (20 nm).

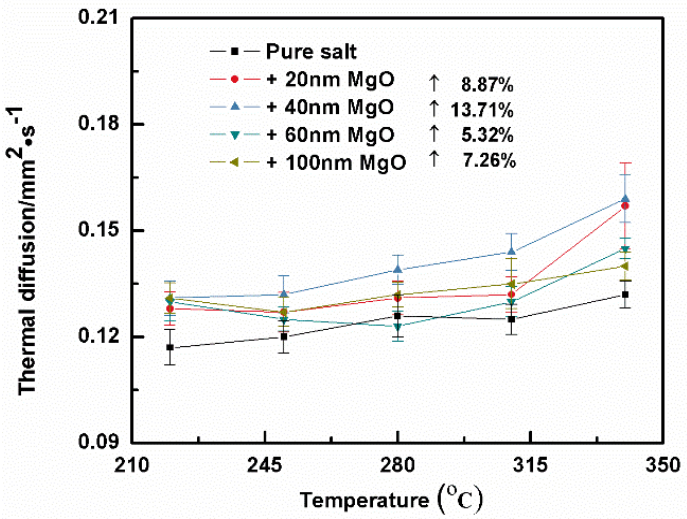

Figure 7. Effects of MgO nanoparticles (with different sizes, 1 wt.%) on the thermal diffusivity.

3.6. Enhanced Thermal Conductivity

From Figure 8, the addition of nano-MgO could dramatically improve the thermal conductivity of the base salt by 11.2–21.2%, which was somewhat positively related to temperature. Brownian motion of nanoparticles can carry high temperature thermal energy and move rapidly towards low temperature regions, and it was considered as the primary factor for thermal conductivity improvement [21]. With the increase of temperature, the micro-perturbations and the diffusivity of heat flow caused by Brownian motion will also be intensified, which can improve the strengthening effect [22]. When nano-MgO with small particle sizes (20 and 40 nm) were added, better improvement effect on thermal conductivity can be achieved by 21%. On the other hand, as nano-MgO with large particle size (100 nm) was added, the enhancement effect was weaker by about 11%. When the same mass percent concentration of nanoparticles was added, the larger the particle size is, the smaller the number is, so the thermal disturbance is weak. This leads to the decrease of its heat transfer characteristics.

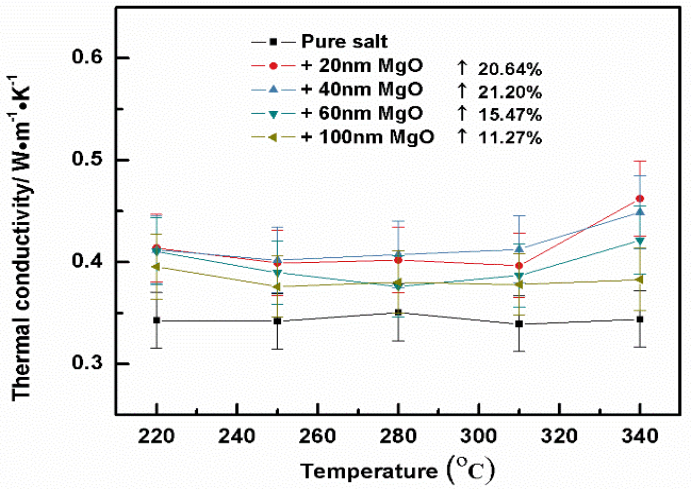

Figure 8. Effects of MgO nanoparticles (with different sizes, 1 wt.%) on the thermal conductivity.

4. Conclusions

In this study, nano-MgO of different particle sizes (20–100 nm) and mass percent concentrations (0.5–2.0wt.%) were dispersed in $LiNO_3$-$NaNO_3$-KNO_3 base salt, and its effects on thermal properties were experimentally investigated. From DSC curves, the introduction of nano-MgO had little effect on its melting temperature, but led to a slight increase in enthalpy of fusion by 2.0–5.5%. For specific heat capacity, the enhancement could reach by 10.6% with optimum size of 20 nm and mass percent concentration of 1 wt.%, and that was remarkably larger than that calculated from classical mixing theory. From SEM graphs, the nubby and punctate microstructures of nanoparticles existed, which could induce the enhancement of specific heat capacity by bringing greater surface area and interfacial energy. Nanoparticles were not obviously influential on density with the largest reinforcement up to 1.15% (1 wt.%, 20 nm). LFA tests demonstrated that the addition of nano-size MgO had a perceptible positive impact on thermal diffusivity. When 1 wt.% MgO were doped in base salt, the nanoparticles of 100 nm size were the optimal group, and the enhancement could be as high as 13.7%. The thermal conductivity remarkably increased with the addition of nanoparticles, and the average thermal conductivity of nanofluid with 1 wt.% nano-MgO of 100 nm was 21.2% higher than that of base salt. Besides, the viscosity of nanofluids slightly increased for 3.3–8.1%. To sum up, the dispersion of nano-MgO into $LiNO_3$-$NaNO_3$-KNO_3 has positive effects on its thermo-physical properties.

Author Contributions: Writing—editing, J.L.; investigation, Z.Z.; methodology, W.W.; project administration, J.D. All authors have read and agreed to the published version of the manuscript.

Funding: This paper is supported by National Natural Science Foundation of China (52036011, U1601215), and Natural Science Foundation of Guangdong Province (2017B030308004).

Institutional Review Board Statement: Not applicable.

Data Availability Statement: Not applicable.

Conflicts of Interest: The authors declare no conflict of interest.

References

1. Lu, J.; Wang, Y.; Ding, J. Nonuniform Heat Transfer Model and Performance of Molten Salt Cavity Receiver. *Energies* **2020**, *13*, 1001. [CrossRef]
2. Liu, J.; He, Y.; Lei, X. Heat-Transfer Characteristics of Liquid Sodium in a Solar Receiver Tube with a Nonuniform Heat Flux. *Energies* **2019**, *12*, 1432. [CrossRef]
3. Dudda, B.; Shin, D. Effect of nanoparticle dispersion on specific heat capacity of a binary nitrate salt eutectic for concentrated solar power applications. *Int. J. Therm. Sci.* **2013**, *69*, 37–42. [CrossRef]

4. Ho, M.X.; Pan, C. Optimal concentration of alumina nanoparticles in molten Hitec salt to maximize its specific heat capacity. *Int. J. Heat Mass Transf.* **2014**, *70*, 174–184. [CrossRef]
5. Wang, B.X.; Zhou, L.P.; Peng, X.F. Surface and Size Effects on the Specific Heat Capacity of Nanoparticles. *Int. J. Thermophys.* **2006**, *27*, 139–151. [CrossRef]
6. Qiao, G.; Cao, H.; Jiang, F.; She, X.; Cong, L.; Liu, Q.; Lei, X.; Alexiadis, A.; Ding, Y. Experimental Study of Thermo-Physical Characteristics of Molten Nitrate Salts Based Nanof luids for Thermal Energy Storage. *ES Energy Environ.* **2019**, *4*, 48–58. [CrossRef]
7. Wei, X.; Yin, Y.; Qin, B.; Wang, W.; Ding, J.; Lu, J. Preparation and enhanced thermal conductivity of molten salt nanofluids with nearly unaltered viscosity. *Renew. Energy* **2020**, *145*, 2435–2444. [CrossRef]
8. Nithiyanantham, U.; González-Fernández, L.; Grosu, Y.; Zaki, A.; Igartua, J.M.; Faik, A. Shape effect of Al2O3 nanoparticles on the thermophysical properties and viscosity of molten salt nanofluids for TES application at CSP plants. *Appl. Therm. Eng.* **2020**, *169*, 114942. [CrossRef]
9. Leal, L.G. On the Effective Conductivity of a Dilute Suspension of Spherical Drops in the Limit of Low Particle Peclet Number. *Chem. Eng. Commun.* **2007**, *1*, 21–31. [CrossRef]
10. Kasaeian, A.; Eshghi, A.T.; Sameti, M. A review on the applications of nanofluids in solar energy systems. *Renew. Sustain. Energy Rev.* **2015**, *43*, 584–598. [CrossRef]
11. Zhao, B.; Ding, J.; Wei, X.; Liu, B.; Lu, J.; Wang, W. Design and thermal stability study of $LiNO_3$-$NaNO_3$-KNO_3 ternary molten salt system. *CIESC J.* **2019**, *70*, 2083–2091.
12. Coscia, K.; Nelle, S.; Elliott, T.; Mohapatra, S.; Oztekin, A.; Neti, S. Thermophysical Properties of $LiNO_3$–$NaNO_3$–KNO_3 Mixtures for Use in Concentrated Solar Power. *J. Sol. Energy Eng.* **2013**, *135*, 034506. [CrossRef]
13. Wang, T.; Viswanathan, S.; Mantha, D.; Reddy, R.G. Thermal conductivity of the ternary eutectic $LiNO_3$–$NaNO_3$–KNO_3 salt mixture in the solid state using a simple inverse method. *Sol. Energy Mater. Sol. Cells* **2012**, *102*, 201–207. [CrossRef]
14. Seo, J.; Shin, D. Size effect of nanoparticle on specific heat in a ternary nitrate ($LiNO_3$–$NaNO_3$–KNO_3) salt eutectic for thermal energy storage. *Appl. Therm. Eng.* **2016**, *102*, 144–148. [CrossRef]
15. Peng, Q.; Ding, J.; Wei, X.; Yang, J.; Yang, X. The preparation and properties of multi-component molten salts. *Appl. Energy* **2010**, *87*, 2812–2817. [CrossRef]
16. Zhu, Y.F.; Lian, J.S.; Jiang, Q. Modeling of the Melting Point, Debye Temperature, Thermal Expansion Coefficient, and the Specific Heat of Nanostructured Materials. *J. Phys. Chem. C* **2009**, *113*, 16896–16900. [CrossRef]
17. Shin, D.; Tiznobaik, H.; Banerjee, D. Specific heat mechanism of molten salt nanofluids. *Appl. Phys. Lett.* **2014**, *104*, 121914. [CrossRef]
18. Hu, Y.; He, Y.; Zhang, Z.; Wen, D. Effect of Al_2O_3 nanoparticle dispersion on the specific heat capacity of a eutectic binary nitrate salt for solar power applications. *Energy Convers. Manag.* **2017**, *142*, 366–373. [CrossRef]
19. Andreu-Cabedo, P.; Mondragon, R.; Hernandez, L.; Martinez-Cuenca, R.; Cabedo, L.; Julia, J.E. Increment of specific heat capacity of solar salt with SiO_2 nanoparticles. *Nanoscale Res. Lett.* **2014**, *9*, 582. [CrossRef]
20. Muñoz-Sánchez, B.; Nieto-Maestre, J.; Veca, E.; Liberatore, R.; Sau, S.; Navarro, H.; Ding, Y.; Navarrete, N.; Juliá, J.E.; Fernández, Á.G.; et al. Rheology of Solar-Salt based nanofluids for concentrated solar power. Influence of the salt purity, nanoparticle concentration, temperature and rheometer geometry. *Sol. Energy Mater. Sol. Cells* **2018**, *176*, 357–373. [CrossRef]
21. Koo, J.; Kleinstreuer, C. A new thermal conductivity model for nanofluids. *J. Nanoparticle Res.* **2005**, *6*, 577–588. [CrossRef]
22. Jang, S.P.; Choi, S.U.S. Role of Brownian motion in the enhanced thermal conductivity of nanofluids. *Appl. Phys. Lett.* **2004**, *84*, 4316–4318. [CrossRef]